4

Channel Identification for OFDM Communication System in Frequency Domain

Lianming Sun
The University of Kitakyushu
Japan

1. Introduction

Orthogonal frequency division multiplexing (OFDM) modulation has excellent performances, for example, strong tolerance against multipath interferences, effective spectral efficiency, high information capacity and simplicity of equalization. Consequently, it has been widely utilized in the services of digital terrestrial broadcasting, asymmetric digital subscriber line (ADSL), local wireless LAN and optical fiber communications. In the transmitter, relay station and receiver, signal processing techniques are used to mitigate the effects caused by various interferences, carrier frequency offset and noise, then to improve the equalization precision of information data. These techniques may achieve the utmost of their effectiveness if the reliable knowledge of the communication channel is applicable. Nevertheless, the prior information of the OFDM channel dynamics is typically unavailable, whereas the practical channel is often time-varying due to the differing propagation paths, scattering and reflection of electric waves. Hence it is necessary to identify the channel model from the observation data and some distinctive structural information inserted in the OFDM signals. In this chapter some channel identification problems as well as the fundamental mathematical tools are discussed, and several frequency domain algorithms are investigated.

Channel information is an essential issue in practical communication systems. It is often obtained by channel identification, which may be performed either in the time domain or in the frequency domain (Giannakis et al., 2000). The identification algorithms in time domain are commonly executed through least mean square (LMS) method, recursive least squares (RLS) method, maximum likelihood (ML) when a known sequence of training symbols transmitted in some specified training styles (Haykin, 2001; Ljung, 1999). When no training sequence can be used for channel identification, the blind (Chi et al., 2006; Ding & Li, 2001) or semi-blind algorithms may use some statical or structured properties of the OFDM signals, for example, the cyclic prefix, the symbol pattern of constellation (Koiveunen et al., 2004). If the spatial information is available, the subspace method is the possible choice (Muquet et al., 2002). These algorithms have been utilized in channel estimation and equalization, and have helped to improve the communication performance in applications of equalization (Giannakis et al., 2000), compensation of frequency offset (Yu & Su, 2004), compensation of nonlinearity distortion (Ding et al., 2004), interference compensation in relay station (Shibuya, 2006; Sun & Sano, 2005).

Nevertheless, in the presence of multipath interferences with long tags, or with the severe restriction that the carriers outside the signal band width do not convey any information

symbols, the time domain algorithms may suffer from either low convergence rate or high computational complexity. Furthermore, if few training sequences can be available for channel estimation, the blind algorithms in the time domain commonly have to employ nonlinear optimization which may converge slowly.

On the other hand, the OFDM signals in base band are managed by Fourier transform and inverse Fourier transform, it implies that the channel identification can also be performed in the frequency domain with the aid of Fourier transform. The advantages of OFDM channel identification in the frequency domain are as follows: Both the transmitted and received signals in base band, and the dynamic channel model can be treated conveniently through Fourier transform in the frequency domain, while fast Fourier transform (FFT) and inverse fast Fourier transform (IFFT) can significantly reduce the computational complexity in channel identification. Additionally, the dynamics of channel model is easily handled in frequency domain without extra computation even for long delay taps, and only simple computation is required for convolution and deconvolution. Furthermore, the scattered pilot symbols assigned at some specified carriers can be more applicable than that in the time domain, and the identification algorithm can easily be combined with equalization, interference cancellation. Hence it is a strong motivation to develop effective channel identification algorithms in the frequency domain.

In this chapter the channel identification is studied in the frequency domain, and several identification algorithms are presented for the OFDM channel working under severe communication environment or restricted identification conditions. Firstly, the frequency properties of both the OFDM signals in base band and the propagation channel used in identification are briefly illustrated, and some structural features of cyclic prefix, constellation of information symbols and scattered pilot symbols are also shown in the frequency domain. Secondly, the fundamentals of identification algorithms are discussed, including the frequency properties of the inter-symbol interference (ISI) and inter carrier interference (ICI), the correlation function and spectral property of various signals in OFDM system, the leakage error of Fourier transform. Then, several identification algorithms are presented, including the batch processing algorithm, recursive algorithm, the usage of pilot symbols, the method to mitigate the affection of equalization errors for the case of low pilot rate. Next, the applications of the identification algorithms are considered for the cases where the multipath interferences have long delay taps, the OFDM signal has severe bandwidth restriction, or the propagation channel has fast fading. Furthermore, their performances of convergence and computational complexity are analyzed, and compared with the methods in the time domain. It is seen that Fourier transform is a powerful mathematical tool in the identification problems of OFDM channel, and the Fourier transform based algorithms demonstrate attractive performance even under some severe communication conditions.

2. Fundamentals in channel identification

2.1 Guard interval

Let the normalized period of OFDM information symbol be denoted as N. As shown in Fig.1, OFDM guard interval (GI) attaches a copy of the effective symbol's tail part to its head as a cyclic prefix when the signal is transmitted. Let the GI length be N_{gi}, then the practical transmission period denoted as N_{tx} becomes to $N_{\text{tx}} = N + N_{\text{gi}}$.

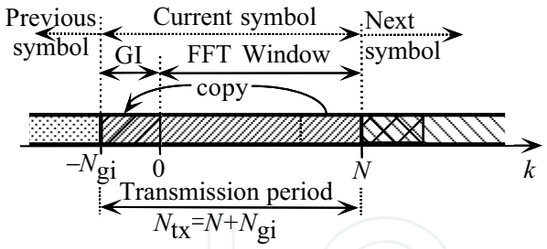

Fig. 1. Guard interval in OFDM signal

2.2 OFDM signals in base band

In the transmission symbol period N_{tx}, the transmitted signal in base band is generated by N-point IFFT as follows

$$d(k) = \sum_{n=-N/2+1}^{N/2} D(n,l) e^{jn\omega_0(k-lN_{tx})}, \text{ for } lN_{tx} - N_{gi} \le k < lN_{tx} + N, \tag{1}$$

where the FFT size N is a power of 2. k and $\omega_0 = 2\pi/N$ are the normalized sampling instant and angular frequency factor, respectively. $D(n,l)$ is the symbol conveyed at the nth carrier in the lth transmission symbol period, and it belongs to a modulation constellation with finite elements.

2.3 Pilot and information symbols

For the purpose of synchronization and equalization, scattered pilot symbols are assigned at the specified carriers, i.e., at these pilot carriers, the transmitted symbols $D(n,l)$ are the known ones at both the transmitter and the receiver, and can be employed in channel identification as well as symbol equalization.

On the other hand, the symbol $D(n,l)$ at information carrier can generally be treated as a random sequence with respect to the carrier number n and symbol period l, i.e.,

$$\lim_{L\to\infty} \frac{1}{L} \sum_{l=1}^{L} D^*(n_1,l) D(n_2, l-l_1) = \bar{D}^2 \delta(n_1 - n_2)\delta(l_1) \tag{2}$$

holds true, where δ is the delta function, * denotes the conjugate complex, $\bar{D}^2$ is the mean square of the constellation, n_1 and n_2 are the carrier numbers, l_1 is an arbitrary integer.

2.4 Multipath channel model

Assume that the received signal in base band under multipath environment can be approximated by

$$y(k) = \sum_{m=0}^{M} r_m(k) + e(k) = \sum_{m=0}^{M} h_m d(k-k_m) + e(k), \tag{3}$$

where $r_m(k)$ is the mth multipath wave to the receiver, h_m is its coefficient, k_m is the delay tap, and $e(k)$ is the additive noise. Correspondingly the channel model can be expressed by z transform as

$$H(z) = h_0 + h_1 z^{-k_1} + h_2 z^{-k_2} + \cdots + h_M z^{-k_M}, \tag{4}$$

where z^{-1} is a backward shift operator, k_M is the longest effective delay tap of interference. Substituting $z = e^{j\omega_0}$ into (4) also yields the frequency response function of the channel model.

3. Identification of multipath channel with long delay taps

When the delay taps of multipath waves are within GI, both equalization and channel identification are easily implemented in OFDM communication (Koiveunen et al., 2004; Wang & Poor, 2003). However, the situation is quite different when the delay taps of some multipath waves exceed GI due to the induced inter-symbol interference (ISI) and inter-carrier interference (ICI) (Suzuki et al., 2002).

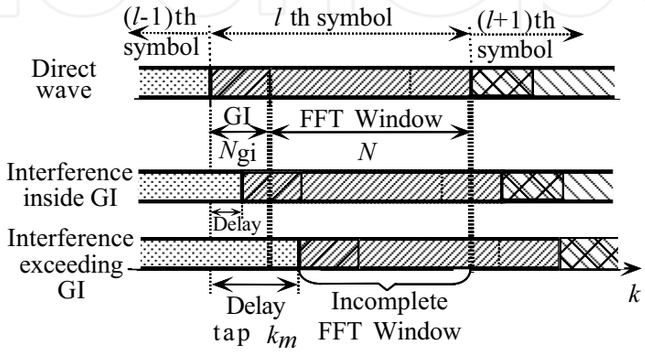

Fig. 2. Multipath interference in OFDM system

3.1 Signal properties used in identification

3.1.1 Interference exceeding GI

Consider the interference $r_m(k)$ with long delay tap k_m exceeding GI. In the lth effective symbol period for $lN_{\text{tx}} \le k < lN_{\text{tx}} + N$, the component of interference with delay tap k_m in Fig.2 is given by

$$r_m(k) = h_m d(k-k_m) = \begin{cases} h_m \sum_{n=-N/2+1}^{N/2} D(n,l-1) e^{jn\omega_0(k-k_m+N_{\text{gi}}-lN_{\text{tx}})} \\ \qquad \text{for } k-k_m-lN_{\text{tx}} < -N_{\text{gi}}, \\ h_m \sum_{n=-N/2+1}^{N/2} D(n,l) e^{jn\omega_0(k-k_m-lN_{\text{tx}})} \\ \qquad \text{for } -N_{\text{gi}} \le k-k_m-lN_{\text{tx}} < N. \end{cases} \tag{5}$$

Performing N-point FFT of $r_m(k)$ within the FFT window for $lN_{\text{tx}} \le k < lN_{\text{tx}} + N$ yields the frequency components of $r_m(k)$. For example, the component corresponding to the nth carrier is expressed by

$$\frac{1}{N}\sum_{k=lN_{\text{tx}}}^{lN_{\text{tx}}+N-1} r_m(k) e^{-jn\omega_0(k-lN_{\text{tx}})} = \frac{1}{N}\sum_{k=0}^{N-1} r_m(k+lN_{\text{tx}}) e^{-jn\omega_0 k}$$
$$= \frac{1}{N}\left(\sum_{k=0}^{k_m-N_{\text{gi}}-1} r_m(k+lN_{\text{tx}}) e^{-jn\omega_0 k} + \sum_{k=k_m-N_{\text{gi}}}^{N-1} r_m(k+lN_{\text{tx}}) e^{-jn\omega_0 k} \right)$$

$$= \frac{h_m}{N} \sum_{k=0}^{k_m - N_{\text{gi}} - 1} \left(\left(\sum_{n_1=-N/2+1}^{N/2} D(n_1, l-1) e^{jn_1\omega_0(k-k_m+N_{\text{gi}})} \right) e^{-jn\omega_0 k} \right)$$

$$+ \frac{h_m}{N} \sum_{k=k_m - N_{\text{gi}}}^{N-1} \left(\left(\sum_{n_1=-N/2+1}^{N/2} D(n_1, l) e^{jn_1\omega_0(k-k_m)} \right) e^{-jn\omega_0 k} \right)$$

$$= \frac{h_m}{N} \sum_{k=0}^{k_m - N_{\text{gi}} - 1} \left(\left(\sum_{n_1=-N/2+1}^{N/2} D(n_1, l-1) e^{jn_1\omega_0(k-k_m+N_{\text{gi}})} \right) e^{-jn\omega_0 k} \right)$$

$$- \frac{h_m}{N} \sum_{k=0}^{k_m - N_{\text{gi}} - 1} \left(\left(\sum_{n_1=-N/2+1}^{N/2} D(n_1, l) e^{jn_1\omega_0(k-k_m)} \right) e^{-jn\omega_0 k} \right)$$

$$+ \frac{h_m}{N} \sum_{k=0}^{N-1} \left(\left(\sum_{n_1=-N/2+1}^{N/2} D(n_1, l) e^{jn_1\omega_0(k-k_m)} \right) e^{-jn\omega_0 k} \right). \tag{6}$$

Following the property of orthogonal basis function of $e^{-jn\omega_0 k}$, the last term in (6) can be written as

$$h_m e^{-jn\omega_0 k_m} D(n, l). \tag{7}$$

Since the term in (7) is only the frequency component at the nth carrier, clearly it still holds the carrier orthogonality. Nevertheless, the first and the second terms in (6), which are the summation within the interval $0 \leq k \leq k_m - N_{\text{gi}} - 1$ of an incomplete FFT window, yield leakage error whose frequency components contaminate all the carriers.

Now consider frequency components of all the multipaths. The orthogonal term at nth carrier becomes to

$$\sum_{m=0}^{M} h_m e^{-jn\omega_0 k_m} D(n, l) = H(e^{jn\omega_0}) D(n, l). \tag{8}$$

On the other hand, the first term in (6) for $k_m > N_{\text{gi}}$ yields ISI, which is the interference from the $(l-1)$th symbol period to the lth period. Let the representation of ISI be denoted as $E_{\text{s}}(n, l)$ in the frequency domain, then it can be expressed by

$$E_{\text{s}}(n, l) = \sum_{m=m_1}^{M} \frac{h_m}{N} \left(\sum_{k=0}^{k_m - N_{\text{gi}} - 1} \left(\sum_{n_1=-N/2+1}^{N/2} D(n_1, l-1) e^{jn_1\omega_0(k-k_m+N_{\text{gi}})} \right) e^{-jn\omega_0 k} \right), \tag{9}$$

where m_1 is the smallest integer such that $k_{m_1} > N_{\text{gi}}$. Moreover, the effect of the second term in (6) leads to $E_{\text{c}}(n, l)$, which is the ICI term given by

$$E_{\text{c}}(n, l) = -\sum_{m=m_1}^{M} \frac{h_m}{N} \left(\sum_{k=0}^{k_m - N_{\text{gi}} - 1} \left(\sum_{n_1=-N/2+1}^{N/2} D(n_1, l) e^{jn_1\omega_0(k-k_m)} \right) e^{-jn\omega_0 k} \right). \tag{10}$$

Let the sum of ISI and ICI be denoted as a leakage error $E(n,l)$. Therefore, the frequency domain expression of the received signal in the lth symbol period is given by

$$Y(n,l) = H(e^{jn\omega_0})D(n,l) + \underbrace{E_{\mathrm{c}}(n,l) + E_{\mathrm{s}}(n,l)}_{E(n,l)} + V(n,l), \tag{11}$$

where $Y(n,l)$ and $V(n,l)$ are the frequency components of the received signal and noise at the nth carrier. It is clear that the leakage error $E(n,l)$ deteriorates the orthogonality of OFDM carriers and will cause large equalization error. A 16 QAM example with high signal to noise ratio (SNR=30dB) is shown in Fig.3. Besides the direct wave, there are two multipath interference waves. Fig.3(a) indicates the result of MMSE equalization where the delay taps are within GI. It is seen that its equalization error is very low, and can be removed by conventional error correction techniques. However, if one of the multipath interference has delay tap exceeding GI, the equalization error significantly increases even under high SNR situations. For example, just one interference with delay tap 1.25 times longer than GI increases the bit error rate (BER) up to 15% in Fig3(b). Therefore, it is important to reduce the influence of $E(n,l)$ to guarantee high communication performance.

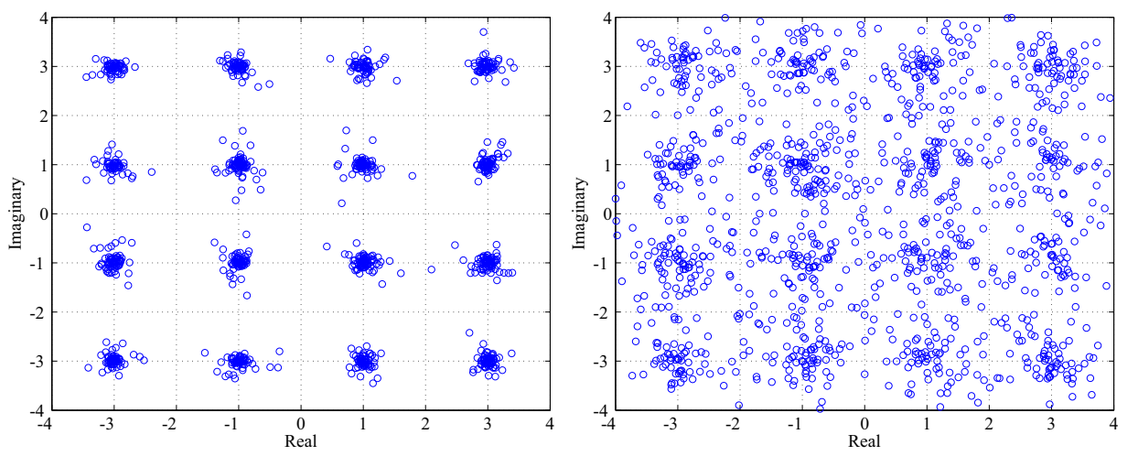

(a) Equalization result when delay taps are within GI

(b) Equalization result when one of the delay taps exceeds GI.

Fig. 3. Examples of equalization with multipath interferences

3.1.2 Expressions of ICI and ISI

It is seen that only the coefficients h_m for $k_m > N_{\mathrm{gi}}$ remain in (9) and (10). Correspondingly, the sub-model of the multipaths exceeding GI can be expressed by z transform as

$$\Gamma(z) = h_{m_1} z^{N_{\mathrm{gi}}+1-k_{m_1}} + h_{m_1+1} z^{N_{\mathrm{gi}}+1-k_{m_1+1}} + \cdots + h_M z^{N_{\mathrm{gi}}+1-k_M}, \tag{12}$$

where $h_{m_1}, h_{m_1+1}, \cdots$ are the coefficients of the multipaths exceeding GI. Then performing inverse Fourier transform of $E_{\mathrm{s}}(n,l)$ in (9) and $E_{\mathrm{c}}(n,l)$ in (10) yields the signals of ISI and ICI in the time domain as

$$\varepsilon_{\mathrm{s}}(k,l) = \Gamma(z) d_{\mathrm{s}}(k,l), \tag{13}$$

$$\varepsilon_{\mathrm{c}}(k,l) = \Gamma(z) d_{\mathrm{c}}(k,l) \tag{14}$$

for $k = 0, 1, \cdots, N-1$, where $d_{\mathrm{s}}(k,l)$ and $d_{\mathrm{c}}(k,l)$ are the corresponding transmitted signals included in (9) and (10). They can be given by

$$d_{\mathrm{s}}(k,l) = \begin{cases} d(k-1+(l-1)N_{\mathrm{tx}}), & \text{for } -N+N_{\mathrm{gi}}+1 \le k \le 0 \\ 0, & \text{for } k > 0 \end{cases}, \tag{15}$$

$$d_{\mathrm{c}}(k,l) = \begin{cases} -d(k-N_{\mathrm{gi}}-1+lN_{\mathrm{tx}}), & \text{for } -N+N_{\mathrm{gi}}+1 \le k \le 0 \\ 0, & \text{for } k > 0 \end{cases}. \tag{16}$$

On the other hand, $E_{\mathrm{s}}(n,l)$ in (9) can be rewritten by

$$E_{\mathrm{s}}(n,l) = \sum_{n_1=-N/2+1}^{N/2} H_{\mathrm{s}}(n,n_1) D(n_1, l-1) \tag{17}$$

in the frequency domain, where $H_{\mathrm{s}}(n,n_1)$ is

$$H_{\mathrm{s}}(n,n_1) = \begin{cases} \sum_{m=m_1}^{M} \frac{h_m}{N} \frac{e^{-jn_1\omega_0(k_m-N_{\mathrm{gi}})} - e^{-jn\omega_0(k_m-N_{\mathrm{gi}})}}{1-e^{-j(n-n_1)\omega_0}}, & \text{for } n \ne n_1, \\ \sum_{m=m_1}^{M} \frac{k_m-N_{\mathrm{gi}}}{N} h_m e^{-jn\omega_0(k_m-N_{\mathrm{gi}})}, & \text{for } n = n_1. \end{cases}$$

Similarly, $E_{\mathrm{c}}(n,l)$ in (10) is approximated by

$$E_{\mathrm{c}}(n,l) = -\sum_{n_1=-N/2+1}^{N/2} H_{\mathrm{c}}(n,n_1) D(n_1,l), \tag{18}$$

where $H_{\mathrm{c}}(n,n_1)$ is given by

$$H_{\mathrm{c}}(n,n_1) = \begin{cases} \sum_{m=m_1}^{M} \frac{h_m}{N} \frac{e^{-jn_1\omega_0 k_m} - e^{-jn\omega_0 k_m} e^{-j(n_1-n)\omega_0 N_{\mathrm{gi}}}}{1-e^{-j(n-n_1)\omega_0}}, & \text{for } n \ne n_1, \\ \sum_{m=m_1}^{M} \frac{k_m-N_{\mathrm{gi}}}{N} h_m e^{-jn\omega_0 k_m}, & \text{for } n = n_1. \end{cases}$$

From (17) and (18), the data in the frequency domain fulfil the following expression

$$\begin{aligned} \mathbf{HD}(l) &= \mathbf{Y}(l) - \mathbf{E}(l) - \mathbf{V}(l) \\ &= \mathbf{Y}(l) - \mathbf{E}_{\mathrm{s}}(l) - \mathbf{H}_{\mathrm{c}}\mathbf{D}(l) - \mathbf{V}(l), \end{aligned} \tag{19}$$

where $\mathbf{Y}(l)$, $\mathbf{D}(l)$, $\mathbf{E}(l)$, $\mathbf{E}_{\mathrm{s}}(l)$ and $\mathbf{V}(l)$ are the vectors of FFT coefficients of the received signal, the information symbols, leakage error, ISI and noise in the lth period, respectively, and

$$\mathbf{H} = \begin{bmatrix} H\left(e^{j(-N/2+1)\omega_0}\right) & & \\ & \ddots & \\ 0 & & H\left(e^{jN/2\omega_0}\right) \end{bmatrix},$$

$$\mathbf{H}_{\mathrm{c}} = \begin{bmatrix} H_{\mathrm{c}}(-N/2+1, -N/2+1) & \cdots & H_{\mathrm{c}}(-N/2+1, N/2) \\ \vdots & \ddots & \vdots \\ H_{\mathrm{c}}(N/2, -N/2+1) & \cdots & H_{\mathrm{c}}(N/2, N/2) \end{bmatrix}.$$

3.1.3 Statistical properties of ICI and ISI

Since $E_{\mathrm{s}}(n,l)$ in (17) is only related to the information symbols in the $(l-1)$th symbol period, then from (2), $D(n,l)$ and $E_{\mathrm{s}}(n,l)$ are uncorrelated, i.e.,

$$\begin{aligned}&\lim_{L\to\infty}\frac{1}{L}\sum_{l=1}^{L}D^*(n,l)E_{\mathrm{s}}(n,l)\\&=\sum_{n_1=-N/2+1}^{N/2}\Big(\lim_{L\to\infty}\frac{1}{L}\sum_{l=1}^{L}D^*(n,l)D(n_1,l-1)\Big)H_s(n,n_1)=0.\end{aligned}\tag{20}$$

Moreover, multiplying $E_{\mathrm{c}}(n,l)$ in (18) by the conjugate information symbol $D^*(n,l)$ and using the results in (2) lead to the following result

$$\begin{aligned}&\lim_{L\to\infty}\frac{1}{L}\sum_{l=1}^{L}D^*(n,l)E_{\mathrm{c}}(n,l)\\&=-\sum_{n_1=-N/2+1}^{N/2}\Big(\lim_{L\to\infty}\frac{1}{L}\sum_{l=1}^{L}D^*(n,l)D(n_1,l)\Big)H_{\mathrm{c}}(n,n_1)\\&=-\bar{D}^2H_{\mathrm{c}}(n,n)=-\bar{D}^2\sum_{m=m_1}^{M}\frac{k_m-N_{\mathrm{gi}}}{N}h_me^{-jnk_m\omega_0}.\end{aligned}\tag{21}$$

Following (21), it is clear that the longer the delay tap k_m, the greater the leakage error is. Therefore, the symbol equalization or interference compensation becomes more difficult.

Furthermore, from (11), the following equation

$$\begin{aligned}\frac{1}{L}\sum_{l=1}^{L}D^*(n,l)Y(n,l)&=H(e^{jn\omega_0})\frac{1}{L}\sum_{l=1}^{L}D^*(n,l)D(n,l)\\&+\frac{1}{L}\sum_{l=1}^{L}D^*(n,l)\Big(E_{\mathrm{s}}(n,l)+E_{\mathrm{c}}(n,l)\Big)+\frac{1}{L}\sum_{l=1}^{L}D^*(n,l)V(n,l)\end{aligned}\tag{22}$$

holds true. Then by using the results of (2), (20) and (21), $\bar{H}(e^{jn\omega_0})$ defined in (23) can be obtained by (22) as follows.

$$\begin{aligned}\bar{H}(e^{jn\omega_0})&=\lim_{L\to\infty}\frac{\frac{1}{L}\sum_{l=1}^{L}(D^*(n,l)Y(n,l))}{\frac{1}{L}\sum_{l=1}^{L}(D^*(n,l)D(n,l))}\\&=H(e^{jn\omega_0})+\lim_{L\to\infty}\frac{\frac{1}{L}\sum_{l=1}^{L}(D^*(n,l)E_{\mathrm{c}}(n,l))}{\frac{1}{L}\sum_{l=1}^{L}(D^*(n,l)D(n,l))}\\&=\sum_{m=0}^{m_1-1}h_me^{-jnk_m\omega_0}+\sum_{m=m_1}^{M}\left(1-\frac{k_m-N_{\mathrm{gi}}}{N}\right)h_me^{-jnk_m\omega_0}.\end{aligned}\tag{23}$$

Denote the IFFT coefficients of $\bar{H}(e^{jn\omega_0})$ as $\bar{h}_0, \bar{h}_1, \bar{h}_2, \cdots$, then the coefficients h_m can be obtained by

$$h_m = \begin{cases} \bar{h}_m, & \text{for } 0 \le k_m \le N_{\text{gi}}, \\ N\bar{h}_m/(N - N_{\text{gi}} + k_m), & \text{for } k_m > N_{\text{gi}}. \end{cases} \tag{24}$$

From (23) and (24), it can be seen that it is possible to estimate $H(e^{jn\omega_0})$ by using the properties of the leakage error even when the channel has long multipath interferences.

3.2 Channel identification algorithm

When several preamble or training symbols are available, (23) and (24) can give a batch channel identification only with computational complexity of $\mathcal{O}(N)$. When no successive training symbols are applicable for channel identification, the pilot symbols could be utilized in some conventional interpolation based channel estimation methods (Coleri et al., 2002; Nguyen et al., 2003). For example, provided that the scattered pilot symbols are assigned at P_nth carrier, then the symbol $D(P_n, l)$ at the pilot carrier P_n is known at the receiver, consequently, the estimation of $\bar{H}(e^{jn\omega_0})$

$$\hat{\bar{H}}(e^{jP_n\omega_0}) = \frac{\frac{1}{L}\sum_{l=1}^{L} D^*(P_n, l)Y(P_n, l)}{\frac{1}{L}\sum_{l=1}^{L} D^*(P_n, l)D(P_n, l)} \tag{25}$$

is obtained at the pilot carrier P_n. As for non-pilot carriers, if the pilot rate is high, a simple linear interpolation yields that

$$\hat{\bar{H}}(e^{jn\omega_0}) = \hat{\bar{H}}(e^{jP_{n,1}\omega_0}) + \frac{n - P_{n,1}}{P_{n,2} - P_{n,1}} \left(\hat{\bar{H}}(e^{jP_{n,2}\omega_0}) - \hat{\bar{H}}(e^{jP_{n,1}\omega_0}) \right), \tag{26}$$

where $P_{n,1}$ and $P_{n,2}$ are the number of two adjacent pilot carriers, $P_{n,1} \le n \le P_{n,2}$. Compared with the linear interpolation, the second order or high order interpolation methods could lead to more smooth interpolation. Furthermore, $\hat{H}(e^{jn\omega_0})$ can be determined by $\hat{\bar{H}}(e^{jn\omega_0})$.

Nevertheless, as mentioned in Section 3.1.1, the components of ICI and ISI contaminate all the carriers, and the frequency response function $H(e^{jn\omega_0})$ varies remarkably when the channel has long multipath interferences, as shown in Fig.4. As a result, neither the interpolation method nor equalization using the frequency selective diversity can yield satisfactory result if the pilot rate is not high enough.

We will consider some new information estimation and channel identification algorithm by making use of multiple receiver antennas and spectral periodograms whose ISI and ICI are compensated by the replica of leakage error.

3.2.1 Diversity of multiple antennas

Commonly, except the symbols at pilot carriers, the information symbols have to be estimated from the received signals for channel identification. Nevertheless, many existing symbol estimation methods cannot work well under the long multipath situations. It is seen that at

the nth carrier where $\left|H(e^{jn\omega_0})\right|$ is small, the orthogonal component in (6) attenuates to such a small value that symbol equalization becomes fragile to the noise and leakage error, even the error correction techniques might fail to correct the equalization errors at the carriers with small magnitude of frequency response. In order to overcome these difficulties, the diversity of multiple receiver antennas is used in the proposed algorithm. Let the total number of antenna elements be Q, correspondingly, the received signal at the qth antenna be denoted as $y_q(k)$, where $1 \leq q \leq Q$. Correspondingly, the frequency response function from the transmitter to the qth antenna is $H_q(e^{jn\omega_0})$, and its sub-model for the exceeding GI part is $\Gamma_q(z)$.

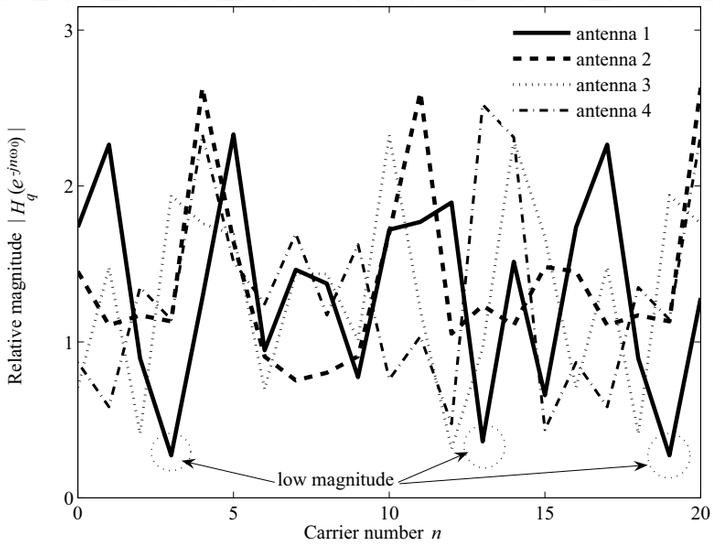

Fig. 4. Example of $|H_q(e^{-jn\omega_0})|$, $q = 1, \cdots, 4$

The relative magnitude of $H_q(e^{jn\omega_0})$ for $1 \leq q \leq 4$ and $0 \leq n \leq 20$ is illustrated in Fig.4. Consider $H_1(e^{-jn\omega_0})$ of the first antenna, notice that at the carriers $n = 3, 13, 19$ marked by circle the low $\left|H_1(e^{-jn\omega_0})\right|$ implies that the symbols are difficult to be estimated by frequency selective diversity of single antenna, since low magnitude of $H_1(e^{jn\omega_0})$ leads to a weak orthogonal component in the received signal $y_1(k)$. On the other hand, $H_2(e^{jn\omega_0})$ has larger magnitude at the carriers marked with circle, and can help the estimation of information symbols.

An approach had been discussed in (Sun et al., 2009) to perform symbol estimation per information carrier by selecting the largest magnitude $\left|H_q(e^{-jn\omega_0})\right|$ from the Q receiver antennas, where it had to perform ICI reduction and symbol estimation iteratively. Next, the more effective estimation approaches without iterative computation will be considered.

3.2.2 Estimation of information symbols

In the lth symbol period, let the frequency component of $y_q(k)$ at the nth carrier be denoted by $Y_q(n, l)$. It is calculated from $y_q(k)$ easily by using FFT algorithm within the FFT window $lN_{\text{tx}} \leq k < lN_{\text{tx}} + N$. From (19), the relation between the symbol vector and received signals

can be expressed by

$$\left(\mathbf{H}_q + \mathbf{H}_{\mathrm{c},q}\right)\mathbf{D}(l) = \mathbf{Y}_q(l) - \mathbf{E}_{\mathrm{s},q}(l) - \mathbf{V}_q(l), \tag{27}$$

where the subscript q indicates the antenna number. Two algorithms are developed to estimate the symbol vector $\mathbf{D}(l)$ in the lth period from the received signals and the estimated channel models.

In the $(l-1)$th symbol period, denote the estimates of information symbol as $\hat{D}(n, l-l)$, the frequency response as $\hat{H}_q(e^{jn\omega_0}, l-1)$, and its sub-model for the part exceeding GI as $\hat{\Gamma}_q(z, l-1)$, respectively. These estimates are used in the estimation of $\hat{D}(n,l)$ and $\hat{H}_q(e^{jn\omega_0}, l)$, and the affection of ISI is mitigated by estimating $\mathbf{E}_{\mathrm{s},q}(l)$ from $\hat{D}(n, l-l)$ and $\hat{\Gamma}_q(z, l-1)$ in (13). The received signal with ISI compensation in the frequency domain is indicated as $\bar{\mathbf{Y}}_q(l) = \mathbf{Y}_q(l) - \mathbf{E}_{\mathrm{s},q}(l)$.

A. Key magnitude selection based approach

Let $q_{\max}(n)$ be the antenna number such that

$$q_{\max}(n) = \arg\max_{q} \left(\left| \hat{H}_q(e^{jn\omega_0}, l-1) + \hat{H}_{\mathrm{c},q}(n,n) \right| \right). \tag{28}$$

It is seen that $|\hat{H}_{q_{\max}(n)}(e^{jn\omega_0}, l-1) + \hat{H}_{\mathrm{c},q_{\max}(n)}(n,n)|$ takes the maximum for $1 \le q_{\max}(n) \le Q$ at the nth carrier so that the strongest orthogonal component is used to estimate the information symbol $D(n,l)$. It means that the influence of ICI and ISI will be decreased through the technique of key magnitude selection (KMS). Define a matrix $\mathbf{H}_{\mathrm{kms}}(l)$ such that the nth diagonal entry is $\hat{H}_{q_{\max}(n)}(e^{jn\omega_0}, l-1) + \hat{H}_{\mathrm{c},q_{\max}(n)}(n,n)$, while the other entries in the nth row are the values of $\hat{H}_{\mathrm{c},q_{\max}(n)}(n, n_1)$. Furthermore, separate $\mathbf{H}_{\mathrm{kms}}(l)$ into the diagonal part $\mathbf{H}_{\mathrm{kms,dg}}(l)$ and the $\mathbf{H}_{\mathrm{kms,nodg}}(l)$. Then the estimate of $\mathbf{D}(l)$ can be given by

$$\hat{\mathbf{D}}(l) = \mathbf{H}_{\mathrm{kms}}^{-1}(l)\bar{\mathbf{Y}}_{\mathrm{kms}}(l) = \left(\mathbf{H}_{\mathrm{kms,dg}}(l) + \mathbf{H}_{\mathrm{kms,nodg}}(l)\right)^{-1}\bar{\mathbf{Y}}_{\mathrm{kms}}(l), \tag{29}$$

where $\bar{\mathbf{Y}}_{\mathrm{kms}}(l)$ is the corresponding vector of $Y_{q_{\max}(n)}(n,l)$. However, the computation of direct inverse $\mathbf{H}_{\mathrm{kms}}^{-1}(l)$ is time-consuming. In the proposed algorithm an approximation of the matrix inverse is considered.

Notice that the magnitude of the diagonal entries in $\mathbf{H}_{\mathrm{kms,dg}}(l)$ is larger than that of $\mathbf{H}_{\mathrm{kms,nodg}}(l)$ in the key magnitude selection, then the inverse $\mathbf{H}_{\mathrm{kms}}^{-1}(l)$ can be approximated by

$$\begin{aligned}
&\mathbf{H}_{\mathrm{kms}}^{-1}(l) = \left(\mathbf{H}_{\mathrm{kms,dg}}(l) + \mathbf{H}_{\mathrm{kms,nodg}}(l)\right)^{-1} \\
&= \left(\mathbf{H}_{\mathrm{kms,dg}}(l)\left(\mathbf{I} + \mathbf{H}_{\mathrm{kms,dg}}^{-1}(l)\mathbf{H}_{\mathrm{kms,nodg}}(l)\right)\right)^{-1} \\
&\approx \left(\mathbf{I} - \left(\mathbf{I} - \mathbf{H}_{\mathrm{kms,dg}}^{-1}(l)\mathbf{H}_{\mathrm{kms,nodg}}(l)\right)\mathbf{H}_{\mathrm{kms,dg}}^{-1}(l)\mathbf{H}_{\mathrm{kms,nodg}}(l)\right)\mathbf{H}_{\mathrm{kms,dg}}^{-1}(l).
\end{aligned} \tag{30}$$

where $\mathbf{H}_{\mathrm{kms,dg}}^{-1}(l)$ is just the reciprocal of the diagonal matrix $\mathbf{H}_{\mathrm{kms,dg}}(l)$. Therefore, the estimate of $\mathbf{D}(l)$ is obtained by multiplication of matrices and vectors, and the estimate of

information symbol $D(n,l)$ at nth carrier can be determined by hard decision, or other error correction techniques (Glover & Grant, 1998).

B. Maximal ratio combination based approach

Define a matrix $\mathbf{H}_{\text{mrc}}(l)$ and a vector $\bar{\mathbf{Y}}_{\text{mrc}}(l)$ whose entries of the nth row vector are the addition as follows

$$\sum_{q=1}^{Q}\left(H_q(e^{-jn\omega_0})+H_{\text{c},q}(n,n)\right)^*\left(\mathbf{H}_q(n)+\mathbf{H}_{\text{c},q}(n)\right), \tag{31}$$

$$\sum_{q=1}^{Q}\left(H_q(e^{-jn\omega_0})+H_{\text{c},q}(n,n)\right)^*\bar{Y}_q(n,l), \tag{32}$$

where $\mathbf{H}_q(n)$ and $\mathbf{H}_{\text{c},q}(n)$ are the nth row vector of $\mathbf{H}_q$ and $\mathbf{H}_{\text{c},q}$, respectively. If the phase of $H_q(e^{-jn\omega_0})+H_{\text{c},q}(n,n)$ is close to the true one, then the diagonal part $\mathbf{H}_{\text{mrc,dg}}(l)$ of $\mathbf{H}_{\text{mrc}}(l)$ will yield the dominate component of $\bar{\mathbf{Y}}_{\text{mrc}}(l)$ and lead to an effect of maximal ratio combination (MRC) (Burke et al., 2005). Therefore, similarly as (29), $\mathbf{D}(l)$ can be estimated by

$$\hat{\mathbf{D}}(l)=\mathbf{H}_{\text{mrc}}^{-1}(l)\bar{\mathbf{Y}}_{\text{mrc}}(l)=\left(\mathbf{H}_{\text{mrc,dg}}(l)+\mathbf{H}_{\text{mrc,nodg}}(l)\right)^{-1}\bar{\mathbf{Y}}_{\text{mrc}}(l), \tag{33}$$

where the inverse of $\mathbf{H}_{\text{mrc}}(l)$ is calculated by a similar approximation as in (30).

Compared with the KMS based approach, the MRC based approach uses all of the received signals' information to reduce the influence of the additive noise, whereas its performance depends on the phase accuracy of $\hat{H}_q(e^{-jn\omega_0})+\hat{H}_{\text{c},q}(n,n)$. A feasible choice is in the first several symbol periods to employ KMS based approach, which does not depend on the phase information so much, then to switch to the MRC based approach after the estimation error decreases to a low level.

3.2.3 Estimation of leakage error

The time domain sequence $\hat{d}(k)$ is calculated through IFFT of $\hat{D}(n,l)$, then $\hat{d}_{\text{c}}(k,l)$ can be obtained by (16). Using the estimation of $\hat{\Gamma}_q(z,l-1)$ and $\hat{d}_{\text{c}}(k,l)$, the values of $\varepsilon_{\text{c},q}(k,l)$ can be estimated by (14) in the time domain first. Consequently, $\hat{E}_{\text{c},q}(n,l)$ can be calculated from FFT of $\varepsilon_{\text{c},q}(k,l)$, and the leakage error $\hat{E}_q(n,l)$ can also be obtained by $\hat{E}_{\text{s},q}(n,l)+\hat{E}_{\text{c},q}(n,l)$.

3.2.4 Estimation of frequency response function

The channel model is estimated from the frequency component $Y_q(n,l)$, the symbol estimate $\hat{D}(n,l)$ and the replica of leakage error $\hat{E}(n,l)$. Consequently, it is important to remove the influence caused by the noise term in $Y_q(n,l)$, the estimation errors of $\hat{D}(n,l)$ and $\hat{E}(n,l)$. The phases of noise and estimation errors are usually random, then their influence can be mitigated through the smoothing effect of spectral periodograms (Pintelon & Schoukens, 2001). In the iteration of lth symbol period, the spectral periodograms $S_{DD}(e^{jn\omega_0},l)$ and $S_{DY}(e^{jn\omega_0},l)$ are defined as follows,

$$S_{DD}(e^{jn\omega_0},l)=\lambda_l S_{DD}(e^{jn\omega_0},l-1)+\hat{D}^*(n,l)\hat{D}(n,l), \tag{34}$$

$$S_{DY,q}(e^{jn\omega_0},l)=\lambda_l S_{DY,q}(e^{jn\omega_0},l-1)+\hat{D}^*(n,l)\left(Y_q(n,l)-\hat{E}_q(n,l)\right) \tag{35}$$

where λ_l is a forgetting factor over the range of $0 < \lambda_l < 1$. It is seen that the effects of noise and estimation errors are reduced when l becomes large. Using the estimates $S_{DD}(e^{jn\omega_0}, l-1)$ and $S_{DY,q}(e^{jn\omega_0}, l-1)$ in the iteration of $(l-1)$th symbol period, as well as the estimates $\hat{D}(n,l)$, $Y_q(n,l)$ and $\hat{E}_q(n,l)$ in the lth iteration, the estimates of (34) and (35) are obtained. Thus the estimate of frequency response function $\hat{H}_q(e^{jn\omega_0}, l)$ can be given by

$$\hat{H}_q(e^{jn\omega_0}, l) = \frac{S_{DY,q}(e^{jn\omega_0}, l)}{S_{DD}(e^{jn\omega_0}, l)}. \tag{36}$$

Moreover, $\hat{\Gamma}_q(z,l)$ can be updated by (12) using IFFT of $\hat{H}_q(e^{jn\omega_0}, l)$. Then let $l = l+1$ for the next iteration.

As mentioned previously, the frequency response function varies remarkably when the interferences have long delay taps. As a result, the side lobes often occur in the impulse response $\hat{h}_m$ of channel model due to the noise, the estimation errors of information symbols and leakage error, etc. Through setting a threshold between main lobe and side lobes, the effect of side lobes can be reduced to improve the convergence performance of channel identification and BER performance of symbol estimation (Hamazumi & Imamura, 2000).

3.2.5 Procedure of channel identification

In the identification algorithm, the estimation of $\hat{D}(n,l)$ is calculated from the received signal compensated by $\hat{E}_s(n,l)$ first, next the leakage error $\hat{E}(n,l)$ is estimated, then the channel frequency response is estimated from the spectral periodograms of the transmitted and received signals. The procedure of proposed algorithm can be summarized as follows.

Step 1. Let the initial values of $\hat{D}(n,0)$, $S_{DY,q}(e^{jn\omega_0}, 0)$, $S_{DD}(e^{jn\omega_0}, 0)$ be 0. Choose the initial values of $\hat{H}_q(e^{jn\omega_0}, 0)$, $\hat{\Gamma}_q(z,0)$, and let the iteration number be $l = 1$.

Step 2. Calculate $Y_q(n,l)$ from the received signal $y_q(k)$ within the FFT window $lN_{\text{tx}} \le k < lN_{\text{tx}} + N$ through FFT.

Step 3. Calculate $d_s(k,l)$ by (15), and $E_{s,q}(n,l)$ by FFT of $\varepsilon_{s,q}(k,l)$ in (13).

Step 4. Estimate $\hat{\mathbf{D}}(l)$ by (29) or (33), and determine $\hat{D}(n,l)$ by hard decision or some error correction techniques, respectively.

Step 5. Calculate $d_c(k,l)$ in (16), furthermore estimate the replica of ICI through FFT of $\hat{\varepsilon}_{c,q}(k,l)$ in (14).

Step 6. Calculate $S_{DY,q}(e^{jn\omega_0}, l)$ and $S_{DD}(e^{jn\omega_0}, l)$ by (34) and (35), respectively.

Step 7. Estimate $\hat{H}_q(e^{jn\omega_0}, l)$ from (36) and update the sub-model $\hat{\Gamma}_q(z,l)$ by (12). Let $l = l+1$, then return to Step 2 to repeat the iterations.

3.3 Algorithm features

The features of the proposed algorithm are summarized as follows.

(1) Periodograms can smooth the power spectra $S_{DY,q}(e^{jn\omega_0}, l)$ and $S_{DD}(e^{jn\omega_0}, l)$ so that the periodograms based identification algorithm can reduce the estimation error of $\hat{H}_q(e^{jn\omega_0}, l)$, which is caused by the estimation errors of $\hat{D}(n,l)$ and $\hat{E}_q(n,l)$, or the noise term in $Y_q(n,l)$ (Pintelon & Schoukens, 2001).

(2) Unlike some other algorithms in the time domain whose performance depends on the total number of parameters to be estimated (Ljung, 1999), the proposed algorithm estimates the frequency response function per carrier from the spectral periodograms and shows good convergence performance even for long impulse response of channel.

(3) By virtue of the multiple antennas' diversity, the stronger orthogonal component is used in KMS or MRC to estimate the information symbols, and it improves the performance of channel identification and symbol estimation significantly compared with the single antenna case.

It is noticed that the purpose of using multiple antennas is just the utilization of the stronger orthogonal component at each carrier, the performance of the proposed algorithm does not depend on the total number of antenna elements as much as the conventional spatial equalizers based on antenna diversity (Higuchi & Sasaoka, 2004; Hori et al., 2003). Moreover, the switching between KMS and MRC improves the algorithm performance under the low pilot rate or low SNR environment, and the proposed algorithm can easily be combined with some error correction techniques to obtain better BER performance.

(4) The forgetting factor is used in periodogram estimation so that the algorithm can also deal with slow time-varying channels. A small forgetting factor has adaptability to quick channel variation and large BER, whereas a large one is used in low SNR environment for spectral smoothing.

(5) When the interference that exceeds GI is strong, the convergence of channel identification and BER performance can be improved by appropriately choosing the side lobe threshold to reduce the influence of side lobes.

(6) The main computation only requires FFT, matrix multiplication, division of periodograms, therefore, the algorithm has less computational complexity and can easily be utilized in the practical applications.

In each iteration, besides the computation of FFT, the proposed algorithm needs the following calculations: $2(k_M - N_{\text{gi}})^2 q$ multiplications to estimate ICI and ISI, about N^2 multiplications and divisions for updating $\mathbf{H}_{\text{kms}}(l)$ or $\mathbf{H}_{\text{mrc}}(l)$, about $2N^2$ multiplications to estimate the information symbols, $(q+1)N$ multiplications to estimate periodograms, qN divisions to estimate the frequency response functions. It is seen that the main computation concentrates on the estimation of information symbols, whereas the channel identification is very simple in the frequency domain. By contrast with the computational complexity of RLS algorithm, besides the estimation of information symbols in RLS algorithm, the recursive identification requires about $\mathcal{O}(k_M^2 N_{\text{tx}})$ multiplications for one symbol period. It is clear that the proposed identification algorithm has less complexity than RLS, especially for large k_M. Though LMS only requires $\mathcal{O}(2k_M N_{\text{tx}})$ multiplications for channel identification, its convergence rate is much slower than RLS (Balakrishnan et al., 2003).

3.4 Numerical simulation examples

3GPP 2.5MHz OFDM transmission with 16QAM modulation is used in the examples where the FFT size $N = 256$, GI length $N_{\text{gi}} = N/4 = 64$ (3GPP, 2006). Moreover, the number of carriers is 256, the total number of receiver antennas is $Q = 2$, and their distance is $1/2$ of the wave length. The noise is assumed as an additive Gaussian white noise.

3.4.1 Example of a simple channel model

Besides the direct wave, there are three multipath interferences in the transmission channel (Higuchi & Sasaoka, 2004; Hori et al., 2003). The coefficients of the waves are illustrated in Table.1. Let the SNR= 20dB. The simulation is performed under 6 conditions of pilot rates:

Wave	Power (dB)	Phase	DOA	Delay tap
Direct	0	0	$\pi/8$	0
Interference 1	-3	$-\pi/6$	$-\pi/4$	$3N_{\rm gi}/4$
Interference 2	-5	$\pi/4$	$\pi/3$	$5N_{\rm gi}/4$
Interference 3	-5	$-\pi/3$	$-\pi/6$	$7N_{\rm gi}/4$

Table 1. Simulation conditions

The successive training symbols are available for identification; the pilot rates are 1/2, 1/4, 1/8, 1/16, respectively; and a severe case where only one pilot carrier is known to remove the ambiguity of channel identification and symbol estimation. At the pilot carrier, the value of $\hat{D}(n,l)$ is given by the corresponding true value of pilot symbol, while at the other carriers, the value of $D(n,l)$ has to be estimated from the received signals. Channel identification is started from the initial values of $\hat{H}(e^{jn\omega_0},0)=1$, $\hat{\Gamma}(z,0)=0$. For the comparison of estimation errors, the square error of channel identification Er_H defined by

$$Er_H = \frac{\sum_q \sum_{n=0}^{N-1} \left| \hat{H}_q(e^{jn\omega_0}) - H_q(e^{jn\omega_0}) \right|^2}{\sum_q \sum_{n=0}^{N-1} \left| H_q(e^{jn\omega_0}) \right|^2}, \tag{37}$$

is illustrated in Fig.5(a), and BER curves of the estimated symbols are illustrated in Fig.5(b), respectively. They show that the algorithm works well even for few pilot carrier cases. In Fig.5(b), BER of the estimated symbols decreases to 0 after several iterations, whereas it is larger than 0.5 at low pilot rate in the first iteration due to the initial value of channel identification is quite different from the true one. It implies that the algorithm converges even under the severe initial conditions. The BER curves are plotted in Fig.5(b) when the channel estimate is used for symbol estimation. It is seen that the good BER performance can be guaranteed if the influence of ISI and ICI caused by the long multipath interferences is compensated by the replica of leakage error.

Since RLS algorithm is often used for channel identification in the previous methods, the results of RLS algorithm are also shown in Fig.5(a) and Fig.5(b) for comparison with the proposed algorithm. They are obtained under the same simulation conditions. In RLS algorithm, the recursion is performed per sampling instant to estimate the parameters of h_m in (3) by using the latest samples of $y(k)$ and $d(k)$, thus RLS updates the estimates $N_{\rm tx}=320$ times during 1 iteration in the proposed algorithm. In Fig.5(a), if several successive training periods are available, i.e., the true values of $d(k)$ can be used for channel identification directly, it is seen that RLS algorithm can yield a small error by using the true $d(k)$ while its computational load is heavier than that of the proposed algorithm. However, when the training symbols are unavailable, $\hat{d}(k)$ has to be estimated for channel identification, the error of $\hat{d}(k)$ deteriorates the identification performance of RLS algorithm. For example, when the pilot rate is 1/2, the convergence of channel identification and the symbol estimation

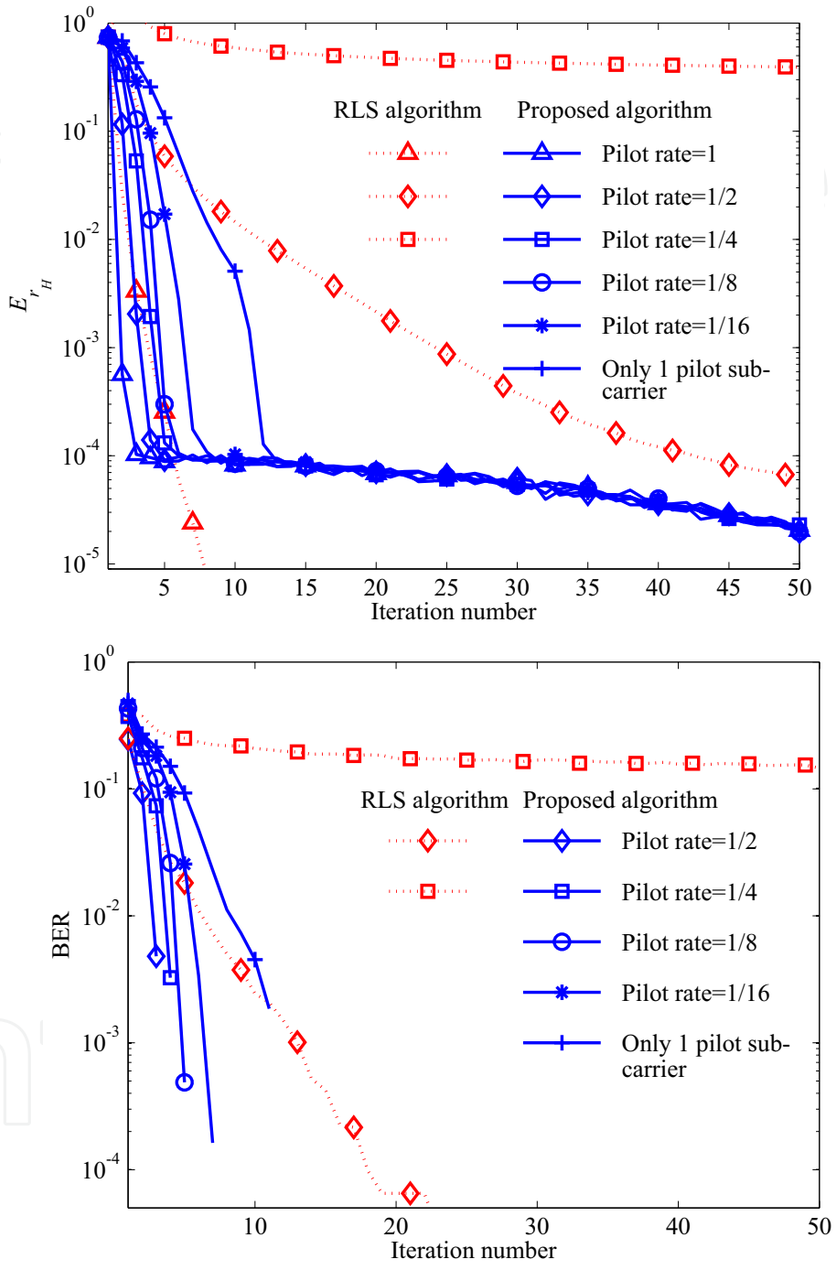

(b) BER of estimated symbols.

Fig. 5. Estimation result (average of 30 simulation runs)

used RLS estimation is much slower than that of the algorithm in frequency domain, and its performance becomes very poor when the pilot rate is 1/4, whereas the proposed algorithm works well since it uses spectral periodograms.

3.4.2 Channel identification versus noise

Let the pilot rate be 1/8, and SNR be changed from 10dB to 40dB, the other conditions be the same as those in Section 3.4.1. Er_H plotted in Fig.6 shows that the proposed algorithm converges even for low SNR conditions.

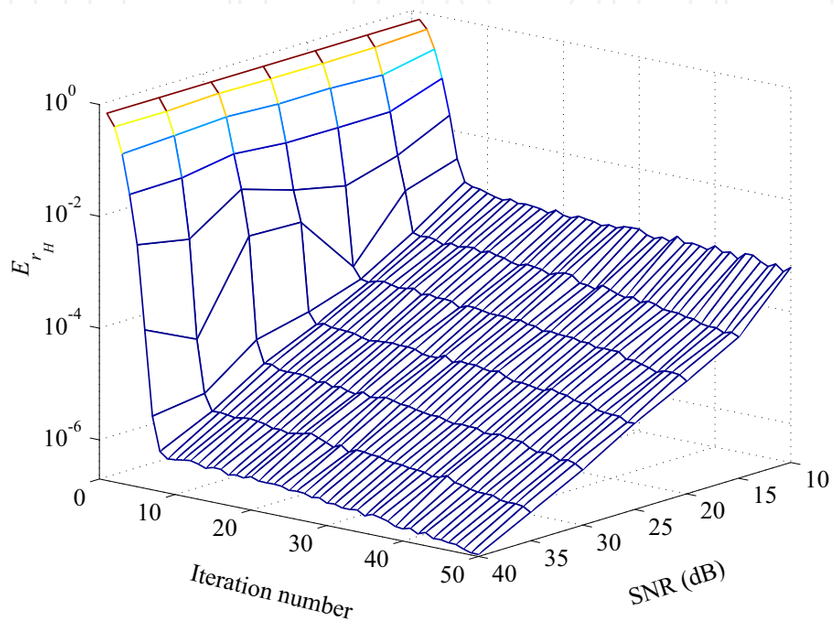

Fig. 6. Channel estimation error versus SNR

3.4.3 Channel identification versus interference power

Let the pilot rate be 1/8, and the power of interference 3 be changed from 0dB to -20dB, the other conditions be the same as those in Section 3.4.1. Er_H and BER versus interference power are illustrated in Fig.7(a) and Fig.7(b), respectively. It is seen that the interferences exceeding GI with high path gain cause severe ICI and ISI, while their information is not so fragile to the side lobes caused by noise, ICI and ISI. Therefore, the convergence of the channel estimation for the interference path with high gain is a little faster than the convergence for the interference with low path gain, as shown in Fig.7(a), and the convergence of channel estimation helps to compensate the influence of ICI and ISI. Though there are two strong multipath interferences exceeding GI, both Er_H and BER are decreased to a considerable low level after just about several iterations.

3.4.4 Channel identification versus total number of antennas

Let the pilot rate be 1/8. In order to investigate the influence of Q on the algorithm performance, the total number Q of antennas is chosen as $Q = 1$, 2, 3 and 4 respectively. The other simulation conditions are the same as those in Section 3.4.1. The curves of Er_H and

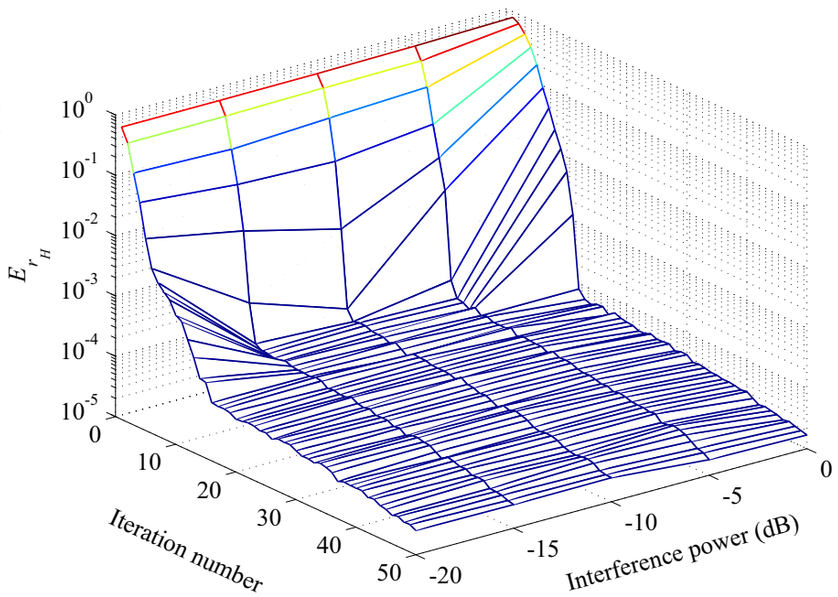

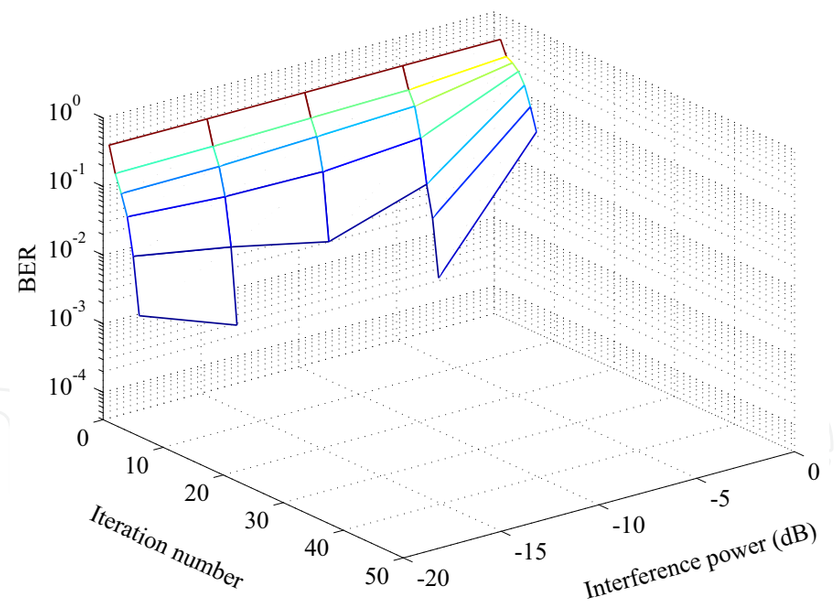

(b) Bit error rate

Fig. 7. Estimation error versus interference power

BER are plotted in Fig.8. If only a single antenna 1 is used for symbol estimation, as illustrated in Fig.4, although the estimation error of $H_1(e^{jn\omega_0})$ decreases to a low level after 10 iterations, the low magnitude of $H_1(e^{jn\omega_0})$ leads to weak orthogonal component in the received signal, as a result, the BER remains high for $Q = 1$. On the other hand, both the errors E_{r_H} and BER for $Q = 2$, 3 and 4 are very low since the strong orthogonal components can be used in symbol estimation, and just 2 antennas can yield good performance in this example. It is seen that though BER is large in the first several iterations, its influence is mitigated in periodograms so that channel identification can provide an effective channel model for equalization.

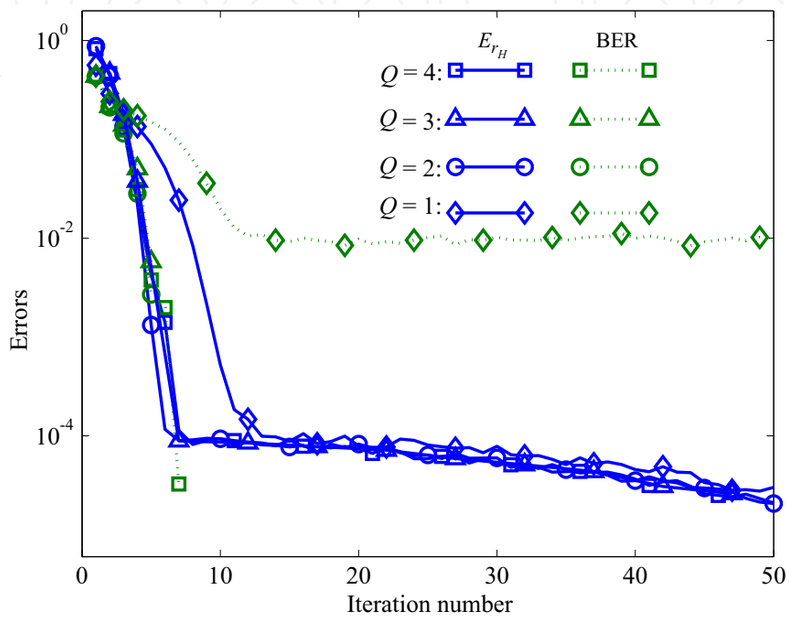

Fig. 8. Channel estimation error and BER versus antenna number Q

3.4.5 Channel identification versus FFT size N

The effect of FFT size N on the channel identification is considered in the simulation. Here N is chosen as 64, 128, 256 and 512, respectively, the GI length is $N_{\text{gi}} = N/4$. Besides the direct path, the delay taps of 3 interference paths are $3N_{\text{gi}}/4$, $5N_{\text{gi}}/4$, $7N_{\text{gi}}/4$, respectively. The coefficients of interference power, phase, DOA are given in Table 1, and the other simulation conditions are the same as those in Section 3.4.1. The channel estimation error E_{r_H} under the 4 cases of FFT size N is illustrated in Fig. 9.

Following the expressions in (9) and (10), or in (17) and (18), it is seen that the effects of ICI and ISI decrease a little with increasing FFT size N in the spectral periodogrames of $S_{DY,q}(e^{jn\omega_0}, l)$. Consequently, the error of channel estimation becomes lower for large N since the effects of side lobe caused by ICI and ISI reduce with increasing FFT size N, and the proposed algorithm yields good BER performance under the given simulation conditions.

3.4.6 Identification of time-varying channel

Let the pilot rate be 1/8, the power, phase and DOA of Interference 3 be changed at every 10 symbol periods so that the channel is time-varying. The power profile is shown in Fig.10(a).

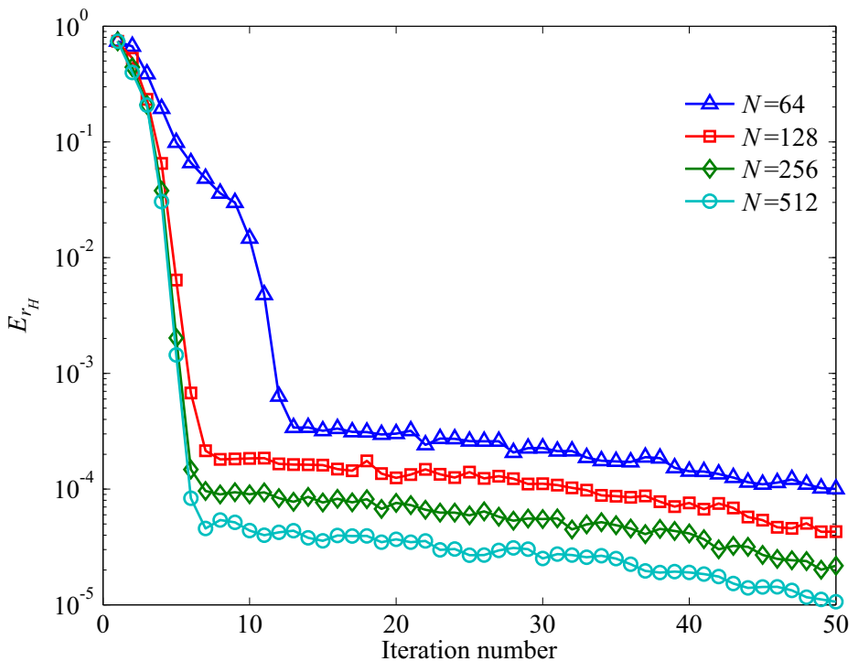

Fig. 9. Channel estimation error versus FFT size N

For the variation of channel, the forgetting factor $\lambda_l = \min\{0.075 \times 1.05^l, 0.75\}$ is used. At the first several iterations, small λ_l is selected to mitigate the influences of high estimated symbols' BER and the effect of side lobes. With decreasing of BER, λ_l is increased gradually to smooth the periodograms. The results of Er_H, BER are illustrated in Fig.10(b). Though the channel varies quickly, the prompt reduction of errors shows that the proposed algorithm can also work well for time-varying channels.

3.4.7 Channel identification of COST 207 model

Let the pilot rate be $1/8$. Assume that the delay profile of the multipath in a hill area is a COST 207 model (European Communities, 1989). There are eleven waves with delay time $0 \leq k_m \leq 10$ and power $e^{-\frac{k_m}{2.5}}$, twenty one waves with delay time $40 \leq k_m \leq 60$ and power $0.7079e^{-\frac{k_m-40}{4}}$, fifteen waves exceeding GI with delay time $72 \leq k_m \leq 96$ and power $0.5623e^{-\frac{k_m-72}{3.6}}$, and $m = 0$ denotes the direct wave. The total power of interferences exceeding GI is -1.29dB. The DOA of multipath waves are generated randomly, and the other conditions are the same as in Section 3.4.1.

As illustrated in Fig.11(a), the received signal suffers from strong multipath interferences, as a result, BER is about 0.4 without interference compensation. In the simulation, the side lobe threshold is chosen as $\max\{0.1 \times 0.98^l, 0.005\}$ to reduce the influence of side lobe. At the first several iterations, a large side lobe threshold is selected, whereas the side lobe threshold is decreased gradually to deal with weak multipath interferences. The corresponding Er_H and BER of estimated symbols are shown in Fig.11(b). Though the channel has strong multipath interferences, Er_H decreases from 1.0 to 0.0025, BER decreases from 0.4 to 0 in about 30 iterations.

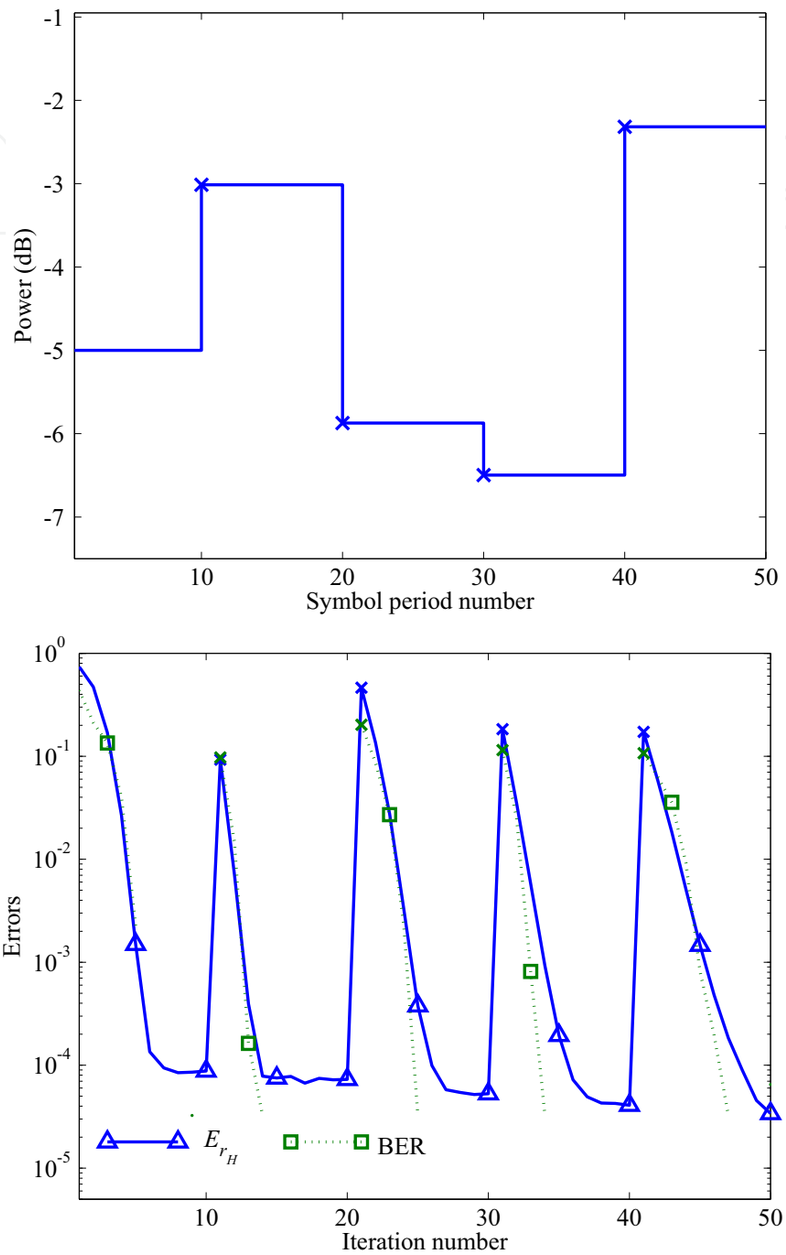

(b) Channel estimation error and BER

Fig. 10. Estimation errors for time-varying channel

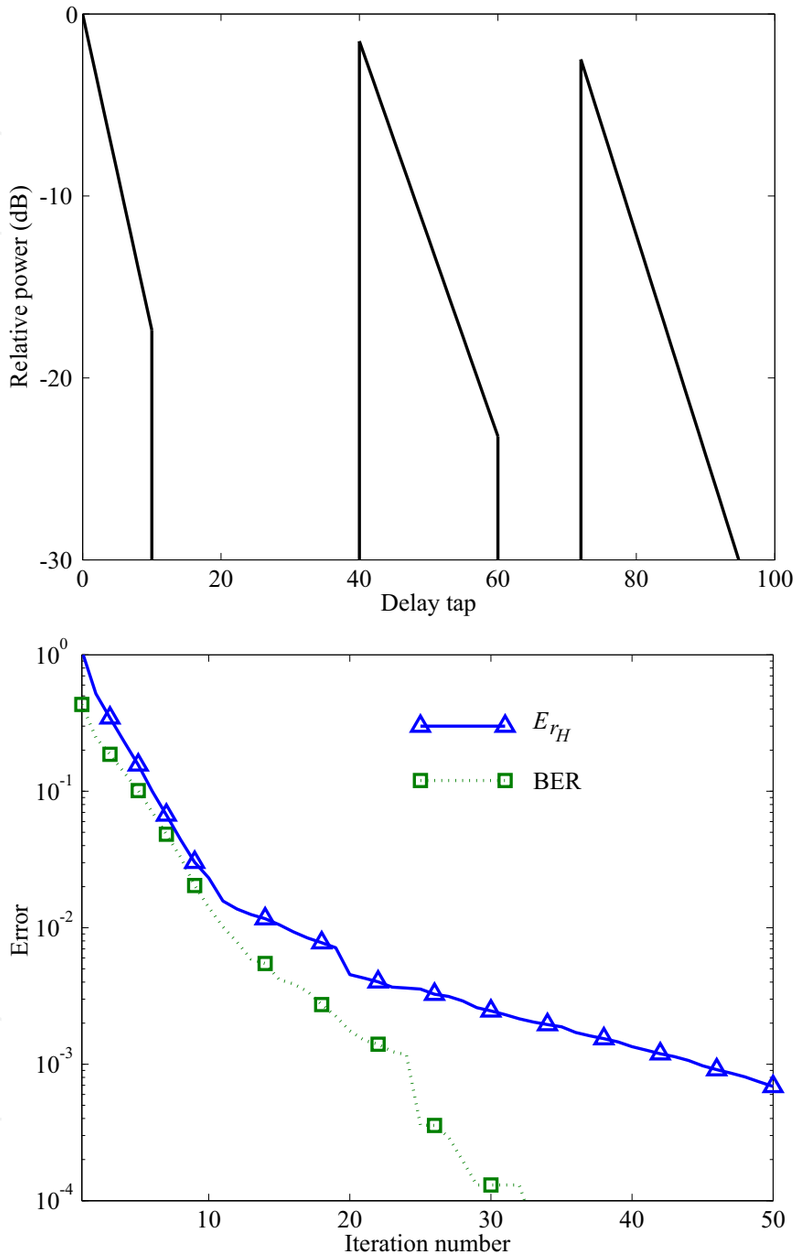

(b) Channel estimation error and BER of estimated symbols

Fig. 11. Estimation errors (average of 30 simulation runs).

4. Identification of channel with limited bandwidth

In some large capacity OFDM systems such as digital terrestrial television broadcasting, the carriers far away from the frequency of central band do not convey any information data in order to simplify the design of filter with sharp cut-off performance and not to interference the adjacent communication channels, thus the transmitted signal is restricted within a specified frequency band. Due to the dynamic modes of the transmission channel cannot be excited beyond the signal band, channel identification becomes a very difficult problem (Ljung, 1999).

On the other hand, if the adaptive algorithms for OFDM system has feedback element, not only the channel information inside the signal band, but also the outside band is important to the processing performance of system stability and convergence rate. When the delay taps are very short and the width of outside band is much narrower than the signal band, extrapolation may exploit a little information outside the signal band from the information inside the band (Hamazumi et al., 2000). This problem had been discussed in the time domain (Sun & Sano, 2005; Ysebaert et al., 2004), however, it is suffered from considerable computational complexity due to the nonlinear optimization or operation of high dimension data matrices. So a frequency domain approach is investigated to decrease the computational complexity (Sun & Sano, 2007).

4.1 Signal bandwidth

In the lth transmission symbol period, the symbol $D(n,l)$ of OFDM signal with limited bandwidth is as follows.

$$D(n,l) = \begin{cases} \text{Symbol data}(\neq 0), & \text{for } |n| \leq N_1 \\ 0, & \text{for } |n| > N_1 \end{cases} \tag{38}$$

where $N_1 < N/2$. It can be seen that the carriers whose distance from the central carrier are more than N_1 do not carry any information data, hence the spectrum of transmitted signal $d(k)$ in an effective symbol period, i.e. $lN_{\text{tx}} \leq k < lN_{\text{tx}} + N$, is limited to $|n| \leq N_1$, whereas the spectral density outside signal band, i.e. for $|n| > N_1$, becomes to 0. It implies that $d(k)$ and its corresponding received signal $y(k)$ for $lN_{\text{tx}} \leq k < lN_{\text{tx}} + N$ do hold little information about the channel dynamics outside the signal band.

4.2 Fourier analysis of specified signals

Two signals are constructed from the original transmitted and received signals as follows:

$$u(k) = d(k - N_{\text{gi}}) - d(k - N_{\text{gi}} - N), \tag{39}$$

$$x(k) = y(k - N_{\text{gi}}) - y(k - N_{\text{gi}} - N). \tag{40}$$

As an example, the signal $u(k)$ is illustrated in Fig.12, where K is an integer satisfying $N_{\text{gi}} < K + N_{\text{gi}} \leq N$, e.g., $K = N/2$. Moreover, the expressions of $u(k)$, $x(k)$ and their relation can also be constructed similarly as $d(k)$ and $y(k)$. From the feature of guard interval, $u(k) = 0$ holds for $lN_{\text{tx}} - N_{\text{gi}} \leq k < lN_{\text{tx}}$. Then substituting (1) into the expression of $u(k)$ yields that

$$u(k) = \sum_{n=-N_1}^{N_1} D(n,l) e^{jn\omega_0(k - lN_{\text{tx}} - N_{\text{gi}})} - \sum_{n=-N_1}^{N_1} D(n,l-1) e^{jn\omega_0(k - lN_{\text{tx}})}$$

$$= \sum_{n=-N_1}^{N_1} \left(D(n,l)e^{-jn\omega_0 N_{\rm gi}} - D(n,l-1) \right) e^{jn\omega_0 (k-lN_{\rm tx})},$$

$$\text{for } lN_{\rm tx} \le k < K + lN_{\rm tx}. \tag{41}$$

Next consider the signal $x(k)$. Let its component corresponding to interference m be denoted

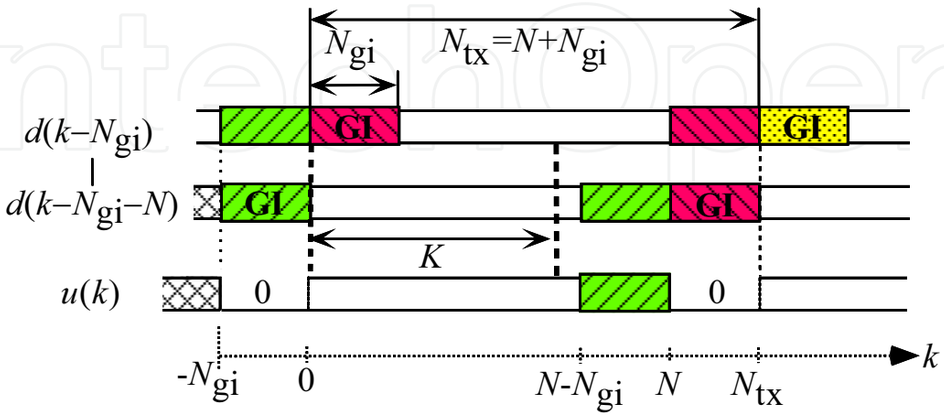

Fig. 12. Illustration of signal $u(k)$

by $x_m(k)$, then omitting the noise term for the simplicity of notation, $x_m(k)$ and $x(k)$ can be expressed by

$$x_m(k) = h_m u(k-k_m), \;\; x(k) = \sum_{m=0}^{M} x_m(k) \tag{42}$$

Moreover, in the lth symbol period, $x_m(k)$ becomes to

$$x_m(k) = \begin{cases} h_m \sum_{n=-N_1}^{N_1} \left(D(n,l)e^{-jn\omega_0 N_{\rm gi}} - D(n,l-1) \right) e^{jn\omega_0 (k-lN_{\rm tx}-k_m)}, \\ \qquad\qquad \text{for } k_m \le k - lN_{\rm tx} < K \\ 0, \qquad\qquad \text{for } 0 \le k - lN_{\rm tx} < k_m \end{cases} \tag{43}$$

On the other hand, let the Fourier transform of $u(k)$ in $lN_{\rm tx} \le k < K + lN_{\rm tx}$ be given by

$$U(n,l) = \sum_{k=lN_{\rm tx}}^{K+lN_{\rm tx}-1} u(k)e^{-jn\omega_0 (k-lN_{\rm tx})} \tag{44}$$

for $n = -N/2+1, \cdots, N/2$, and similarly the Fourier transform of $x(k)$, then the following frequency properties of signals $u(k)$ and $x(k)$ satisfy the following equation:

$$H(e^{jn\omega_0})U(n,l) = X(n,l) + \sum_{m=0}^{M} h_m \left(E_{m,1}(n,l) + E_{m,2}(n,l) \right) \tag{45}$$

where $E_{m,1}(n,l)$ and $E_{m,2}(n,l)$ are the leakage terms to the nth frequency point from the other components, the nth frequency component itself, respectively. Their theoretical

representations are expressed by

$$E_{m,1}(n,l)=e^{-jn\omega_0 k_m}\sum_{\substack{\bar{n}=-N_1\\ \bar{n}\neq n}}^{N_1}\Big(D(\bar{n},l)e^{-j\bar{n}\omega_0 N_{\mathrm{gi}}}-D(\bar{n},l-1)\Big)\cdot\frac{e^{-j(n-\bar{n})\omega_0(K-k_m)}-e^{-j(n-\bar{n})\omega_0 K}}{1-e^{-j(n-\bar{n})\omega_0}}, \tag{46}$$

$$E_{m,2}(n,l)=k_m e^{-j\omega_0 k_m}\Big(D(n,l)e^{-jn\omega_0 N_{\mathrm{gi}}}-D(n,l-1)\Big). \tag{47}$$

4.3 Spectra estimation

Let the power spectrum of $u(k)$ be estimated by

$$S_{UU}(n,l)=\frac{1}{l}\sum_{l_1=1}^{l}U^*(n,l_1)U(n,l_1), \tag{48}$$

and $S_{UE_{m,1}}(n,l)$ and $S_{UE_{m,2}}(n,l)$ are defined in the similar formula. Then $S_{UU}(n,l)$ can be approximated as

$$S_{UU}(n,l)\approx 2\overline{D}^2\sum_{\substack{\bar{n}=-N_1\\ \bar{n}\neq n}}^{N_1}\frac{1-\cos(n-\bar{n})\omega_0 K}{1-\cos(n-\bar{n})\omega_0}+2K^2\overline{D}^2$$

for $|n|\leq N_1$ when l is large enough, and

$$S_{UU}(n,l)\approx 2\overline{D}^2\sum_{\bar{n}=-N_1}^{N_1}\frac{1-\cos(n-\bar{n})\omega_0 K}{1-\cos(n-\bar{n})\omega_0} \tag{49}$$

for $N_1<|n|<N/2$. Meanwhile, $S_{UE_{m,1}}(n,l)$ satisfies

$$S_{UE_{m,1}}(n,l)\approx\overline{D}^2\sum_{\substack{\bar{n}=-N_1\\ \bar{n}\neq n}}^{N_1}\left(\frac{1-e^{-j(n-\bar{n})\omega_0 K}}{1-\cos(n-\bar{n})\omega_0}\left(e^{-jn\omega_0 k_m}-e^{-j\bar{n}\omega_0 k_m}\right)\right). \tag{50}$$

Furthermore, the spectral leakage error $S_{UE_{m,2}}(n,l)$ for $|n|\leq N_1$ is

$$S_{UE_{m,2}}(n,l)\approx 2e^{-jn\omega_0 k_m}\overline{D}^2 K k_m, \tag{51}$$

while for $N_1<|n|<N/2$ it turns to

$$S_{UE_{m,2}}(n,l)=0. \tag{52}$$

Following (45), the relation between spectra of $u(k)$, $x(k)$ and the frequency property $H(e^{jn\omega_0})$ is summarized in (53):

$$H(e^{jn\omega_0})S_{UU}(n,l)\approx S_{UX}(n,l)+\sum_{m=0}^{M}h_m\Big(S_{UE_{m,1}}(n,l)+S_{UE_{m,2}}(n,l)\Big). \tag{53}$$

Using the symbol estimation of $D(n,l)$, the signals $d(k)$ as well as $u(k)$ are estimated. Then, $S_{UU}(n,l)$ and $S_{UX}(n,l)$ in (53) can be estimated from $u(k)$ and $x(k)$ directly. On the other hand, from (50)-(52), the terms of spectral leakage error $S_{UE_{m,1}}(n,l)$ and $S_{UE_{m,2}}(n,l)$ can be calculated beforehand without using observation data and the information of channel dynamics. Consequently, it is possible to estimate the channel property outside the signal band from signals $u(k)$ and $x(k)$ if $S_{UX}(n,l)$ is compensated by $S_{UE_{m,1}}(n,l)$ and $S_{UE_{m,2}}(n,l)$.

On the other hand, when the channel is time-varying, a forgetting factor λ can be used to estimate $S_{UU}(n,l)$ and $S_{UX}(n,l)$

$$S_{UU}(n,l) = \lambda S_{UU}(n,l-1) + U^*(n,l)U(n,l), \tag{54}$$

$$S_{UX}(n,l) = \lambda S_{UX}(n,l-1) + U^*(n,l)X(n,l) \tag{55}$$

respectively, where $0 < \lambda < 1$.

4.4 Channel identification algorithm

Following (53), the estimation of channel model can be deduced as

$$\hat{H}(e^{jn\omega_0}) = \frac{S_{UX}(n,l)}{S_{UU}(n,l)} + \sum_{m=0}^{M} \hat{h}_m \frac{S_{UE_{m,1}}(n,l) + S_{UE_{m,2}}(n,l)}{S_{UU}(n,l)}. \tag{56}$$

Notice that the estimates $\hat{h}_m$, the coefficients of IFFT of $\hat{H}(e^{jn\omega_0})$, the estimation can be performed in the following iterative form as

$$\hat{H}^{(i+1)}(e^{jn\omega_0}) = \frac{S_{UX}(n,l)}{S_{UU}(n,l)} + \sum_{m=0}^{M} \hat{h}_m^{(i)} \frac{S_{UE_{m,1}}(n,l) + S_{UE_{m,2}}(n,l)}{S_{UU}(n,l)}, \tag{57}$$

where i is the iteration number, and $\hat{h}_m^{(0)}$ can be chosen as the coefficients of $S_{UX}(n,l)/S_{UU}(n,l)$. When the channel dynamics does not vary too fast, the recursive estimation can also be given by using the estimates $\hat{h}_m^{(l-1)}$, which are estimated in the last symbol period:

$$\hat{H}^{(l)}(e^{jn\omega_0}) = \frac{S_{UX}(n,l)}{S_{UU}(n,l)} + \sum_{m=0}^{M} \hat{h}_m^{(l-1)} \frac{S_{UE_{m,1}}(n,l) + S_{UE_{m,2}}(n,l)}{S_{UU}(n,l)}. \tag{58}$$

The main numerical computation in the identification algorithm is just FFT to estimate the signal $u(k)$, power spectra $S_{UU}(n,l)$, $S_{UX}(n,l)$, division of $\left(S_{UE_{m,1}}(n,l) + S_{UE_{m,2}}(n,l)\right)$ and $S_{UU}(n,l)$, while the two leakage error terms can be pre-calculated, division of $S_{UX}(n,l)$, and $S_{UU}(n,l)$, IFFT $\hat{H}(e^{jn\omega_0})$ to calculate $\hat{h}_m$. Furthermore, the computational complexity does not increase too much even though the interference delay taps get longer. So the identification algorithm can be easily implemented, and combined with other adaptive processing techniques.

On the other hand, $\hat{H}^{(}e^{jn\omega_0})$ inside the signal band can also be given by the spectra of $S_{DY}(n,l)$ and $S_{DD}(n,l)$

$$\hat{H}^{(}e^{jn\omega_0}) = \frac{S_{DY}(n,l)}{S_{DD}(n,l)}, \text{ for } \left|n\right| \leq N_1, \tag{59}$$

where $S_{DY}(n,l)$ and $S_{DD}(n,l)$ are calculated from the received signal $y(k)$ and the symbol estimates $\hat{D}(n,l)$ without using $\left(S_{UE_{m,1}}(n,l)+S_{UE_{m,2}}(n,l)\right)$. Furthermore, if the channel has not too long multipath interferences, interpolating channel information from the pilot carriers to their adjacent carriers is applicable to channel identification inside the signal band, and may reduce the influence caused by the estimation error of information symbols $D(n,l)$.

4.5 Numerical simulation examples

In the simulation, the OFDM information symbols $D(l,n)$ are 64QAM, the FFT/IFFT length is $N = 2048$, the guard interval is $N_{\text{gi}} = N/4$, and $N_1 = 600$. It means that the number of active carriers is 1201, and the signal band is only about 3/5 of the full band width, hence identification of such an OFDM channel is a very difficult problem. There are 6 symbol transmission periods per signal frame, and 200 scattered pilot carriers are distributed uniformly in the first and fourth symbol periods (3GPP, 2006). Let K be chosen as $K = N/2$, the SNR is 15dB.

As shown in Fig.13, the signal $u(k)$ has spectral power density of 10^{-3} outside the signal band. Compared with the original spectrum of $d(k)$ whose magnitude is 0 at the carriers for $|n| > N_1$, the information over the entire frequency band can be extracted from $u(k)$ though the spectral power density outside the band is a little lower than the inside part. It implies that it is possible to identify the dynamics of channel even outside the signal band.

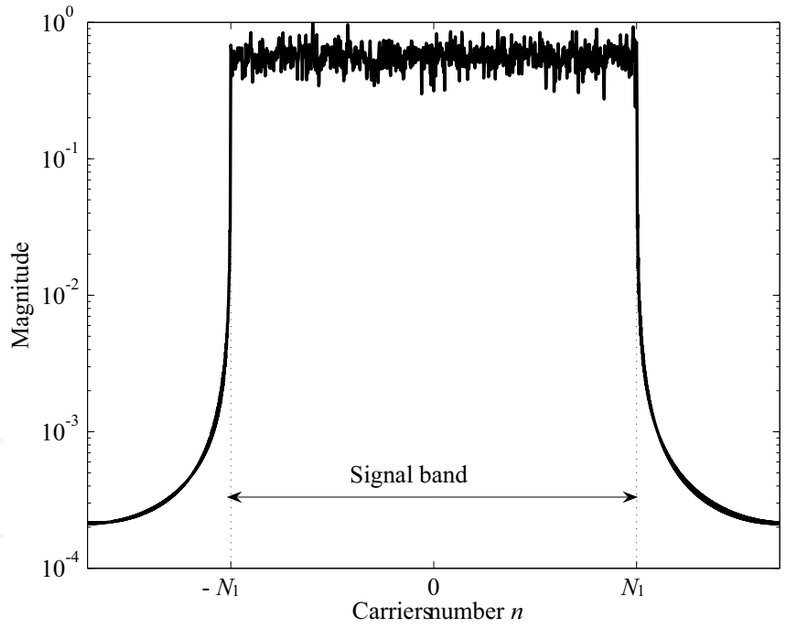

Fig. 13. Spectrum of $u(k)$

The true frequency property of $H(e^{jn\omega_0})$, where the longest effective delay tap $k_M = 100$ is used in channel estimation. The estimates after 50 iterations are plotted in Fig.14. It illustrates that the estimate is very close to the true one even outside the signal band, though the transmitted signal $d(k)$ has severe band limitation. As a comparison, the channel is also identified by conventional methods using RLS and LMS, and the results show that though

both RLS and LMS have estimated the channel property inside the signal band, they cannot provide satisfactory identification outside the signal band.

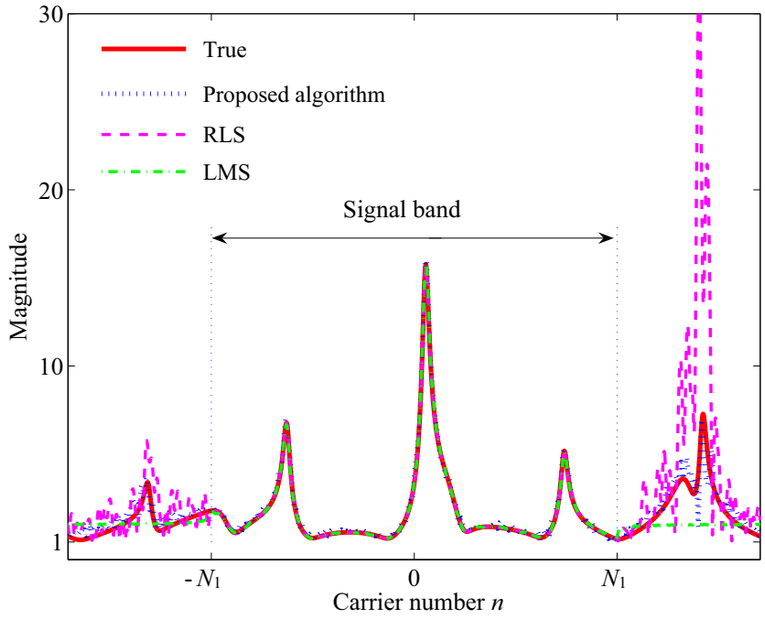

Fig. 14. Frequency property of communication channel

The estimation errors outside the signal band under various noise environments are illustrated in Fig.15, where the error is evaluated by

$$E_{H,\text{out}} = \frac{\sum_{N_1<|n|<\frac{N}{2}} \left|\hat{H}(e^{jn\omega_0}) - H(e^{jn\omega_0})\right|^2}{\sum_{N_1<|n|<\frac{N}{2}} \left|H(e^{jn\omega_0})\right|^2}. \tag{60}$$

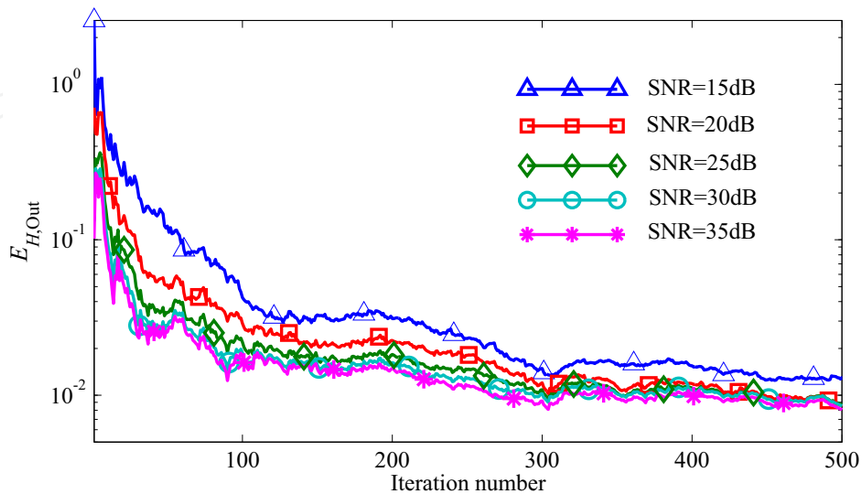

Fig. 15. Estimation error versus different SNR

It can be seen that even for low SNR, the estimation error successfully reduces to a low level just by tens iterations, and the estimated channel model can be applied to design adaptive filters for the OFDM system.

5. Conclusions

Channel identification using Fourier transform has been studied in this chapter. Since the OFDM transmitted signals in base band are generated through discrete Fourier transform, both the transmitted and received signals are easily managed in the frequency domain through Fourier transform. Consequently, the identification problem of OFDM channels could be solved in the frequency domain. Two channels have been investigated: the channel with long multipath interferences; and the transmitted signals with severe band limitation, where the conventional time domain methods cannot offer effective estimation. Firstly the properties of OFDM signals and the structural information have been analyzed in the frequency domain, then the relations of channel model and available information extracted from the observation data and structural information have been induced. Based on these relations, the frequency domain algorithms for OFDM channel identification have been developed, and the techniques have also been investigated to improve the identification accuracy, to deal with the time-varying channel and to reduce the computational complexity. It has been illustrated that the proposed frequency domain algorithms have better performance than the conventional time domain methods under the severe identification conditions considered in these problems, and the numerical results have demonstrated the effectiveness of Fourier transform in the channel identification applications. The algorithms work for the MIMO OFDM systems, and the estimation for OFDM channel with frequency offset are under further research work.

6. References

3GPP (2006). 3GPP TR 25.814 (release 7), *Technical report*, 3rd Generation Partnership Project. URL: *www.3gpp.org/ftp/Specs/html-info/TSG-WG–r1.htm*

Balakrishnan, J., Martin, R. & Johson, J. C. (2003). Blind, adaptive channel shortening by sum-squared auto-correlation minimization (SAM), *IEEE Trans. Signal Processing* 51(12): 3086–3093.

Burke, J., Zeidler, J. & Rao, B. (2005). CINR difference analysis of optimal combining versus maximal ratio combining, *IEEE Trans. Wireless Communications* 4(1): 1–5.

Chi, C., Feng, C., Chen, C. & Chen, C. (2006). *Blind Equalization and System Identification*, Springer.

Coleri, S., Ergen, M. & Bahai, A. (2002). Channel estimation techniques based on pilot arrangement in OFDM systems, *IEEE Trans. Broadcasting* 48(3): 223–229.

Ding, L., Zhou, T., Morgan, D., Ma, Z., Kenney, J., Kim, J. & Giardina, D. (2004). A robust digital baseband predistortion constructed using memory polynomials, *IEEE Trans. Commun.* pp. 159–165.

Ding, Z. & Li, Y. (2001). *Blind Equalization and Identification*, Marcel Dekker, Inc.

European Communities (1989). COST 207, digital land mobile radio communications, final report, *Technical report*, Commission of the European Communities.

Giannakis, G., Hua, Y., Stoica, P. & Tong, L. (2000). *Signal Processing Advances in Wireless and Mobile Communications,* Vol.1*: Trends in Channel Estimation and Equalization*, Prentice-Hall, Englewood Cliffs, NJ.

Glover, I. & Grant, P. (1998). *Digital Communications*, Prentice Hall.

Hamazumi, H., Imamura, K., Iai, N., Shibuya, K. & Sasaki, M. (2000). A study of a loop interference canceller for the relay stations in an SFN for digital terrestrial broadcasting, *GLOBECOM'00: IEEE Global Telecommunications Conference*, San Francisco, pp. 167–171.

Hamazumi, T. & Imamura, K. (2000). Coupling canceller, *Technical report*, NHK Science & Technology Research Laboratories.

Haykin, S. (2001). *Adaptive Filter Theory*, 4th edn, Prentice Hall.

Higuchi, K. & Sasaoka, H. (2004). Adaptive array suppressing inter symbol interference based on frequency spectrum in OFDM systems, *IEICE Trans. Commun.* J87-B: 1222–1229.

Hori, S., Kikuma, N. & Inagaki, N. (2003). MMSE adaptive array suppressing only multipath waves with delay times beyond the guard interval for fixed reception in the OFDM systems, *IEICE Trans. Commun.* J86-B: 1934–1940.

Koiveunen, V., Enescu, M. & Sirbu, M. (2004). Blind and semiblind channel estimation, *in* K. E. Barner & G. R. Arce (eds), *Nonlinear Signal Processing and Image Processing*, CRC Press, pp. 257–332.

Ljung, L. (1999). *System Identification – Theory for the User*, Prentice Hall, Upper Saddle River, NJ.

Muquet, M., Courville, M. & Duhamel, P. (2002). Subspace-based blind and semiblind channel estimation for OFDM systems, *IEEE Trans. Signal Processing* 50(7): 1699–1712.

Nguyen, V., Winkler, M., Hansen, C. & Kuchenbecker, H. (2003). Channel estimation for OFDM systems in case of insufficient guard interval length, *Proc. 15th International Conference on Wireless Communications*, Alberta, Canada.

Pintelon, R. & Schoukens, J. (2001). *System Identification–A Frequency Domain Approach*, IEEE Press.

Shibuya, K. (2006). Broadcast-wave relay technology for digital terrestrial television broadcasting, *Proceedings of the IEEE* 94(1): 269–273.

Sun, L. & Sano, A. (2005). Channel identification for SFN relay station with coupling wave in OFDM systems, *IEICE Trans. Fundamental* J88-A(9): 1045–1054.

Sun, L. & Sano, A. (2007). Channel identification and applications to OFDM communication systems with limited bandwidth, *Proc. 15th European Digital Signal Processing Conference*, Poznan, Poland.

Sun, L., Sano, A., Sun, W. & Kajiwara, H. (2009). Channel identification and interference compensation for OFDM system in long multipath environment, *Signal Processing* 89: 1589–1601.

Suzuki, N., Uehara, H. & Yokoyama, M. (2002). A new OFDM demodulation method with variable-length effective symbol and ICI canceller, *IEICE Trans. Fundamental* E85-A(12): 2859–2867.

Wang, X. & Poor, H. (2003). *Wireless Communication Systems- Advanced Techniques for Signal Reception*, Prentice Hall.

Ysebaert, G., Pisoni, F., Bonavetura, M., Hug, R. & Moonen, M. (2004). Echo cancellation in DMT-receivers: Circulant decomposition canceller, *IEEE Trans. Signal Processing* 52(9): 2612–2624.

Yu, J. & Su, Y. (2004). Pilot assisted ML frequency-offset estimation for OFDM systems, *IEEE Trans. on Communication* 52(11): 1997–2008.

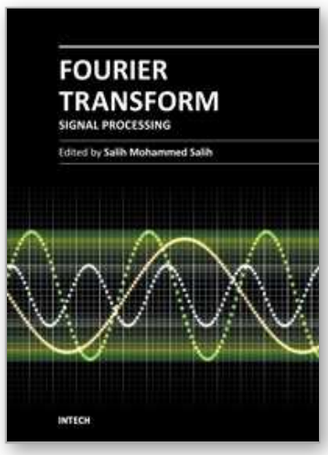

Fourier Transform - Signal Processing

Edited by Dr Salih Salih

ISBN 978-953-51-0453-7
Hard cover, 354 pages
Publisher InTech
Published online 11, April, 2012
Published in print edition April, 2012

The field of signal processing has seen explosive growth during the past decades; almost all textbooks on signal processing have a section devoted to the Fourier transform theory. For this reason, this book focuses on the Fourier transform applications in signal processing techniques. The book chapters are related to DFT, FFT, OFDM, estimation techniques and the image processing techqniques. It is hoped that this book will provide the background, references and the incentive to encourage further research and results in this area as well as provide tools for practical applications. It provides an applications-oriented to signal processing written primarily for electrical engineers, communication engineers, signal processing engineers, mathematicians and graduate students will also find it useful as a reference for their research activities.

INTECH
open science | open minds

InTech Europe
University Campus STeP Ri
Slavka Krautzeka 83/A
51000 Rijeka, Croatia
Phone: +385 (51) 770 447
Fax: +385 (51) 686 166
www.intechopen.com

InTech China
Unit 405, Office Block, Hotel Equatorial Shanghai
No.65, Yan An Road (West), Shanghai, 200040, China
中国上海市延安西路65号上海国际贵都大饭店办公楼405单元
Phone: +86-21-62489820
Fax: +86-21-62489821

IntechOpen